nanomaterials

MDPI

Article

Bio-Inspired Design of Superconducting Spiking Neuron and Synapse

Andrey E. Schegolev [1], Nikolay V. Klenov [2,3], Georgy I. Gubochkin [2,4], Mikhail Yu. Kupriyanov [1] and Igor I. Soloviev [1,3,*]

[1] Skobeltsyn Institute of Nuclear Physics, Lomonosov Moscow State University, 119991 Moscow, Russia; tanuior@gmail.com (A.E.S.); mkupr@pn.sinp.msu.ru (M.Y.K.)
[2] Faculty of Physics, Moscow State University, 119991 Moscow, Russia; nvklenov@mail.ru (N.V.K.); gubochkin.gi19@physics.msu.ru (G.I.G.)
[3] Faculty of Physics, Lobachevsky State University of Nizhny Novgorod, 603950 Nizhny Novgorod, Russia
[4] Russian Quantum Center, 100 Novaya Street, Skolkovo, 143025 Moscow, Russia
* Correspondence: igor.soloviev@gmail.com

Abstract: The imitative modelling of processes in the brain of living beings is an ambitious task. However, advances in the complexity of existing hardware brain models are limited by their low speed and high energy consumption. A superconducting circuit with Josephson junctions closely mimics the neuronal membrane with channels involved in the operation of the sodium-potassium pump. The dynamic processes in such a system are characterised by a duration of picoseconds and an energy level of attojoules. In this work, two superconducting models of a biological neuron are studied. New modes of their operation are identified, including the so-called bursting mode, which plays an important role in biological neural networks. The possibility of switching between different modes in situ is shown, providing the possibility of dynamic control of the system. A synaptic connection that mimics the short-term potentiation of a biological synapse is developed and demonstrated. Finally, the simplest two-neuron chain comprising the proposed bio-inspired components is simulated, and the prospects of superconducting hardware biosimilars are briefly discussed.

Keywords: bio-inspired neuron; spiking neural networks; neuromorphic systems; synapse plasticity; Josephson effect; superconductivity

check for updates

Citation: Schegolev, A.E.; Klenov, N.V.; Gubochkin, G.I.; Kupriyanov, M.Y.; Soloviev, I.I. Bio-Inspired Design of Superconducting Spiking Neuron and Synapse. *Nanomaterials* **2023**, *13*, 2101. https://doi.org/10.3390/nano13142101

Academic Editor: Do Hwan Kim

Received: 15 June 2023
Revised: 11 July 2023
Accepted: 17 July 2023
Published: 19 July 2023

Copyright: © 2023 by the authors. Licensee MDPI, Basel, Switzerland. This article is an open access article distributed under the terms and conditions of the Creative Commons Attribution (CC BY) license (https://creativecommons.org/licenses/by/4.0/).

1. Introduction

The cybernetic brain is an old dream of science fiction writers, the embodiment of artificial consciousness created in the image and likeness of man. Despite the remarkable progress of neuroscience in the understanding of the structure and principles of the human brain [1–11] and the improvement of technology and the development of the physical sciences, the cybernetic brain is still science fiction, although this fiction is closer to reality than it was half a century ago.

Inspired attempts to make this dream come true have resulted in a number of steps towards its realisation, such as the development of synaptic chips by large international companies (IBM [12], Google [13], Intel [14] and Qualcomm [15]) as well as by leading scientific organisations [16–18]; the creation of auditory and visual implants to restore hearing and vision [19–24]; the development of machine learning methods [25–32], including methods that enable people who have lost the ability to move or speak to communicate their thoughts using the brain–computer interface [33]; and, of course, the discovery of the hidden mechanisms of the human brain [34–37].

Spiking neural networks (SNNs) are a recognised class of neural models that most closely mimic the biological activity of nerve tissue, encoding information by spike sequences, allowing synaptic plasticity and learning [38–40]. SNN implementation is in high demand, both for the high-speed simulation of biological neural activity in living tissue,

and for real-time systems needed to create and improve bi-directional brain–computer interfaces [33,41].

There are several hardware implementations of bio-inspired SNN. Neuromorphic chips based on silicon or silicon nitride can achieve greater processing power and problem-solving efficiency than general-purpose processors. In addition, semiconductor technology is well understood, affordable, and has a well-developed technology base and convenient interfaces with external devices [41,42]. However, such a traditional approach results in a large number of transistors in the model (realistic from a biological point of view), relatively low performance and high power consumption. Memristors have properties suitable for mimicking biological synapses but need to be coupled [16,43,44] to spiking neurons based on CMOS circuits, and therefore the whole system suffers from the problems described above. The methods of integrated photonics, which have become widespread lately, provide elements with sub-nanosecond characteristic time scales and greater energy efficiency than their semiconductor counterparts [45,46]. Superconducting technologies can be used to build the fastest and most energy-efficient analogue of a biological neuron. A simple superconducting ring, which does not conduct a magnetic field due to the Meissner–Oxenfeld effect, can play the role of a cell membrane. Weak places in the ring (Josephson junctions, *JJs*), through which magnetic flux quanta can pass, act as analogues of channels for the entry/exit of ions in the operation of a sodium–potassium pump. The time dynamics of the voltage across the Josephson junction during the passage of a quantum is very similar to the typical action potential of a bio-neuron. However, the characteristic time scale here is picoseconds, and the energy dissipated is a fraction of aJ [47–59]. An additional advantage of the superconducting platform is the possibility to investigate the peculiarities of "quantum" decision making [60] by utilising proven quantum-computing systems [61].

In this article, we study the dynamic processes in the simplest Josephson bio-inspired neuron with two Josephson junctions ($2JJ$, see Figure 1a) [47] and identify new operation modes that have biological analogues. In particular, we focus on the bursting mode. For the modified bio-inspired neuron with three Josephson junctions ($3JJ$, see Figure 1b) [62], we reveal the possibility of switching between operation modes in situ on chip. Finally, we propose a modification of synaptic connections that allows synaptic plasticity, an analogue of short-term potentiation (STP). Numerical simulations confirm the validity of the proposed solutions.

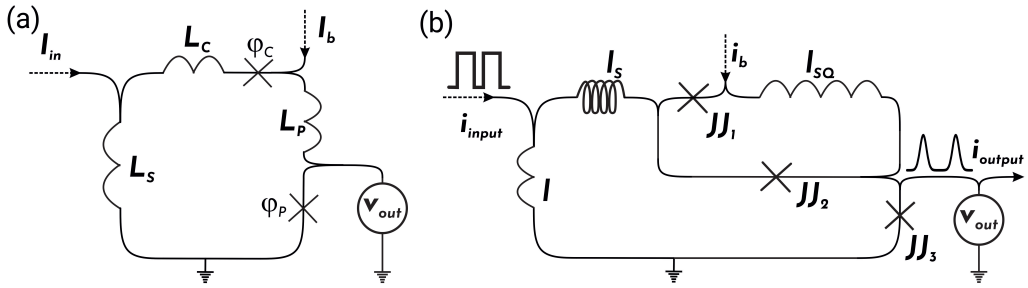


Figure 1. (**a**) Circuit diagram of $2JJ$ neuron from the work [47] and (**b**) schematic representation of modified spiking neuron ($3JJ$ neuron).

2. $2JJ$ and $3JJ$ Neurons

2.1. Research Methods

The modelling of all systems considered below: $2JJ$ and $3JJ$ neurons; axons and different synapses were based on the solution of systems of differential equations for Josephson phases in the frame of the resistively shunted junction (RSJ) model [63]. The state of a Josephson junction is determined by its phase, which serves as a generalised coordinate for the considered nonlinear oscillatory system. The phase time derivative is the voltage normalised with respect to the Josephson junction characteristic value V_C. The fall of this phase across an inductor corresponds to the magnetic flux normalised with respect to the value of the magnetic flux quantum, Φ_0. The input (and output) of magnetic flux

quantum into a "superconducting cell" is accompanied by the appearance of a biosimilar voltage pulse (spike) at the Josephson junction.

The equations for the $2JJ$ neuron, shown in Figure 1a, are as follows:

$$\begin{cases} i_{JJ_c} = i_{in} \cdot \Lambda_s - \lambda(\phi_c + \phi_p) - i_b \cdot \Lambda_p, \\ i_{JJ_p} = i_{in} \cdot \Lambda_s - \lambda(\phi_c + \phi_p) - i_b \cdot (1 - \Lambda_p). \end{cases} \quad (1)$$

Here, $i_{JJ_{c,p}}$ are currents flowing through the "control" (JJ_c) and "pulse" (JJ_p) Josephson junctions, having the phases ϕ_c and ϕ_p, respectively; i_{in} is an input current for the $2JJ$ neuron; $\lambda = (l_s + l_c + l_p)^{-1}$, where $l_{s,p,c} = 2\pi L_{s,p,c} I_C / \Phi_0$; $\Lambda_{s,p} = l_{s,p} \cdot \lambda$; and i_b is a bias current. All currents are normalised by the critical current of the pulse JJ, I_{CC}. The time is normalised with respect to the inverse plasma frequency, $\omega_p^2 = 2\pi I_{CC} / \Phi_0 C$, where C is a capacitance of the pulse Josephson junction. The currents through the Josephson junctions in the circuit can be expressed as

$$i_{JJ_p} = \ddot{\phi}_p + \Gamma \dot{\phi}_p + \sin \phi_p, \quad (2)$$

$$i_{JJ_c} = \eta \cdot (\ddot{\phi}_c + \Gamma \dot{\phi}_c + \sin \phi_c), \quad (3)$$

where $\Gamma^2 = \Phi_0 / 2\pi I_{CC} R_N^2 C$ is a damping parameter, and η is a geometric factor reflecting the ratio of the cross-sectional areas of the control and pulse Josephson junctions ($\eta = A_c / A_p$, the critical current and capacitance of a Josephson junction are assumed to scale linearly with its cross-sectional area).

The equations for the $3JJ$ neuron, see Figure 1b, are as follows:

$$\begin{cases} i_{JJ_1} = -i_b - (\phi_1 - \phi_2) / l_{SQ}, \\ i_{JJ_2} = i_b + (\phi_1 - \phi_2) / l_{SQ} + i_{in} \cdot \lambda l - \lambda \cdot (\phi_2 + \phi_3), \\ i_{JJ_3} = i_b + i_{in} \cdot \lambda l - \lambda(\phi_2 + \phi_3) - i_{out}, \end{cases} \quad (4)$$

where $\lambda = (l + l_s)^{-1}$, all inductances (l, l_s and l_{SQ}) are normalised by $\Phi_0 / 2\pi I_C$, I_C is the third junction (JJ_3) critical current, and i_{out} is an output neuron current. In ω_p-normalisation, the currents through the Josephson junctions in the circuit can be expressed as follows:

$$i_{JJ_1} = \ddot{\phi}_1 + \Gamma \dot{\phi}_1 + \sin \phi_1, \quad (5)$$

$$i_{JJ_2} = \eta \cdot (\ddot{\phi}_2 + \Gamma \dot{\phi}_2 + \sin \phi_2), \quad (6)$$

$$i_{JJ_3} = \ddot{\phi}_3 + \Gamma \dot{\phi}_3 + \sin \phi_3, \quad (7)$$

where Γ is also the damping parameter, and η is responsible for the ratio of cross-sectional areas of the 2nd and 3rd Josephson junctions ($\eta = A_2 / A_3$). We also assume that the critical currents of JJ_1 and JJ_3 are equal.

2.2. Features of the $2JJ$ *and* $3JJ$ *Neurons*

A detailed analysis of the dynamic processes in terms of the greatest biosimilarity (in the framework of the Hodgkin-Huxley model [64]) even in a simple $2JJ$ neuron revealed four main regimes or *modes* of operation. These include the *dead mode*, corresponding to a neuron that does not respond to input stimuli; the *injury mode*, where only some of the input stimuli generate a biosimilar response at the output; the *regular mode*, where any standard input stimulus generates a biosimilar voltage response at the output; and the *bursting mode*, where a standard input stimulus leads to the generation of sequential (bursts) of biosimilar pulses [65–68]. Another regime of operation, the *non-biological mode*, is not the main mode of neuron operation, but it is nevertheless the case for this circuit, characterised by free output pulse generation without any external influence ($I_{in} = 0$) under the bias current, I_b, applied.

From a biophysical point of view, the specific mode of operation is determined by the relationship between the input (corresponding to the JJ_c) and output (corresponding to the

JJ_p) channel conductances. In our analogy with the sodium–potassium pump, the JJ_c junction corresponds to the efflux of K^+ ions from the cell, while the JJ_p junction corresponds to the influx of Na^+ ions (triggers neuron depolarisation). The higher the critical current of the junction, the lower the corresponding channel conductance. The evolution of processes in the neuron also depends on the bias current that support the "excitation" of the neuron and the parameter Γ, which determines the rate of decay of free current oscillations in the Josephson junctions, as well as the dissipation in the neuron model.

Figure 2a shows that in the $2JJ$ neuron, all main modes can only be achieved if the geometric factor η is about and above unity. Figure 2c–f illustrate the voltage behaviour at the Josephson junction, simulating the "ion output" for the regular, bursting, dead and injury modes, respectively.

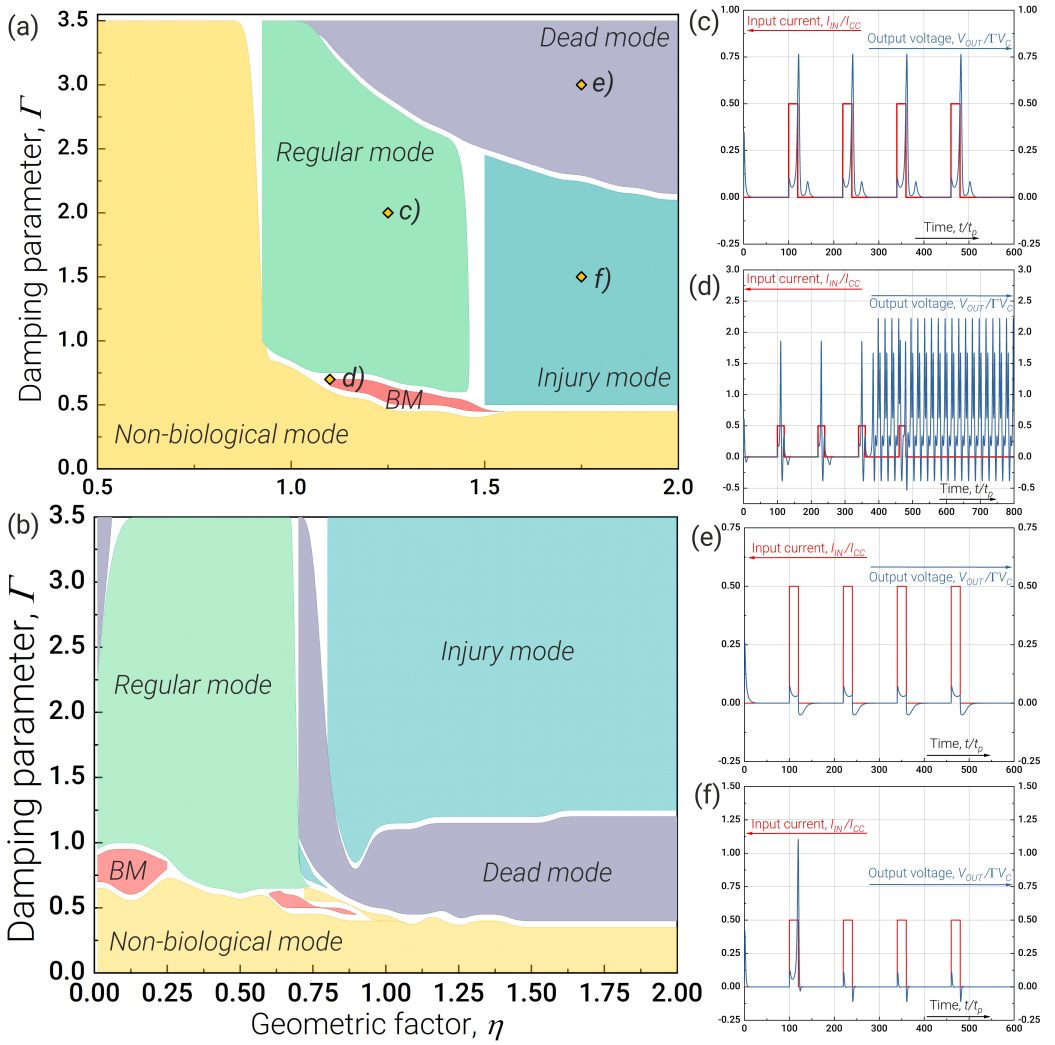


Figure 2. Ranges of parameters for bio-inspired neuron operating modes for damping parameter Γ and geometric factor η for (**a**) $2JJ$ neuron [47] (see Figure 1a) and (**b**) $3JJ$ neuron (see Figure 1b). (**c**–**f**) Panels correspond to different operating modes—(**c**) regular, (**d**) bursting, (**e**) dead and (**f**) injury—of the $2JJ$ neuron (which are qualitatively similar to the operating modes of the $3JJ$ neuron), marked by yellow diamonds in (**a**). *The non-biological mode* is understood as the dynamics of an artificial neuron that has no analogues in its biological counterpart. The parameters of the $2JJ$ neuron are as follows: $l_S = l_P = 5$, $i_b = 1.9$. The parameters of the $3JJ$ neuron: $l_S = 3.85$, $l = 5$, $i_b = 1.9$, $I_{C1}/I_{C3} = 1$. The neuron was excited by the input rectangular pulses with level equal to the $A_{input} = 0.5$ and pulse duration $\tau = 20t_P$.

Regular mode is a typical neuron cell operation mode with an adequate response to external influence and the proper form of output spikes. Areas corresponding to the *regular* mode are marked in green (Figure 2) and the typical proper response to the external influence is demonstrated in Figure 2c. The generation of spikes in this regime is associated with the sodium–potassium pump in living nerve cells, altering the ionic balance and the action potential within them. *Dead mode* is also the typical neuron cell operation mode in cases when a nerve tissue is actually damaged, for example, by certain drugs or toxic substances. Such cells are "deaf" to external influences and unable to process signals. Physically, this means no voltage spikes on the pulse Josephson junction when it is externally excited by the current pulses.

Injury mode is a transition mode between regular and dead modes, respectively. Injury mode is an incorrect mode of neuron operation when the output does not correspond to the expected regular mode of operation: the neuron responds with only one output spike, whereas it ignores the rest of the external current pulses. *Bursting mode* is a typical and very important mode of neuron cell operation [69,70] characterised by the generation of a series or *bursts* of spikes in response to a single stimulating current pulse. Such behaviour may be the result of the complex interaction of neurons in the network, as well as a consequence of internal processes in a neuron. It plays an important role in synaptic plasticity [65,66], the synchronisation of large groups of neurons [71], the detection of frequency features of input stimuli [72], information coding [73,74] and the reliability of synaptic transmission [65,75], which may be crucial for processing important stimuli [76].

In *non-biological mode*, the level of the bias current I_b is sufficient to switch the Josephson junctions of the $2JJ$ neuron to the resistive state and, as a result, to the persistent generation of spikes. From a biological point of view, such a situation is equivalent to the uncontrolled entry of salt ions from a surrounding medium into a nerve cell. Significantly, at the parameter plane, this mode corresponds to a small attenuation in the system or a violation of the balance between the input and output channels for the magnetic flux quanta (relatively small values of JJ_c critical current).

To increase the ability to control the throughput of the input channel, we propose to replace JJ_c with a two-Josephson junction superconducting interferometer. Figure 1b shows that this interferometer contains JJ_1 and JJ_2. We find all the operating modes described above for the $2JJ$ neuron for the modified $3JJ$ neuron as well.

The main advantage of the $3JJ$ neuron is that its operating mode is easier to control. A comparison of Figure 3a,b shows that the $3JJ$ neuron has a significantly larger parameter range (see light blue areas in figures), in which switching between all operating modes is possible solely by controlling the bias current. By choosing parameters for the $2JJ$ neuron partly from [47] and partly from Figure 2a ($l_S = l_P = 5$, $\Gamma = 0.65$) at a fixed value of η, we can switch between all main modes by varying the bias current i_b in a narrow range. For the given parameters, this region lies in the range of η from 1.4 to 1.5 and covers only small parts of the bursting and regular mode regions. At the same time, for the $3JJ$ neuron ($l_S = 3.85$, $l = 5$, $\Gamma = 0.8$), we can also switch between all operating modes due to bias current: for the chosen parameters, this range lies in the range of η from 0.65 to 1.0 and covers large parts of the *bursting*, *regular* (twice), *dead* (twice) and *injury* (twice) modes. The appearance of a periodic structure in the parameter plane as a function of i_b is associated with the quantisation of the magnetic flux in the circuits of the scheme.

Furthermore, the $3JJ$ neuron can be made controllable using identical Josephson junctions, and this design tolerates larger variations in physical parameters of the circuit elements. For the technological spread typical of modern digital Josephson circuits [77], we obtain a relatively small offset of the described operating modes on the parameter plane. However, the essence of the phenomena described in the article remains the same.

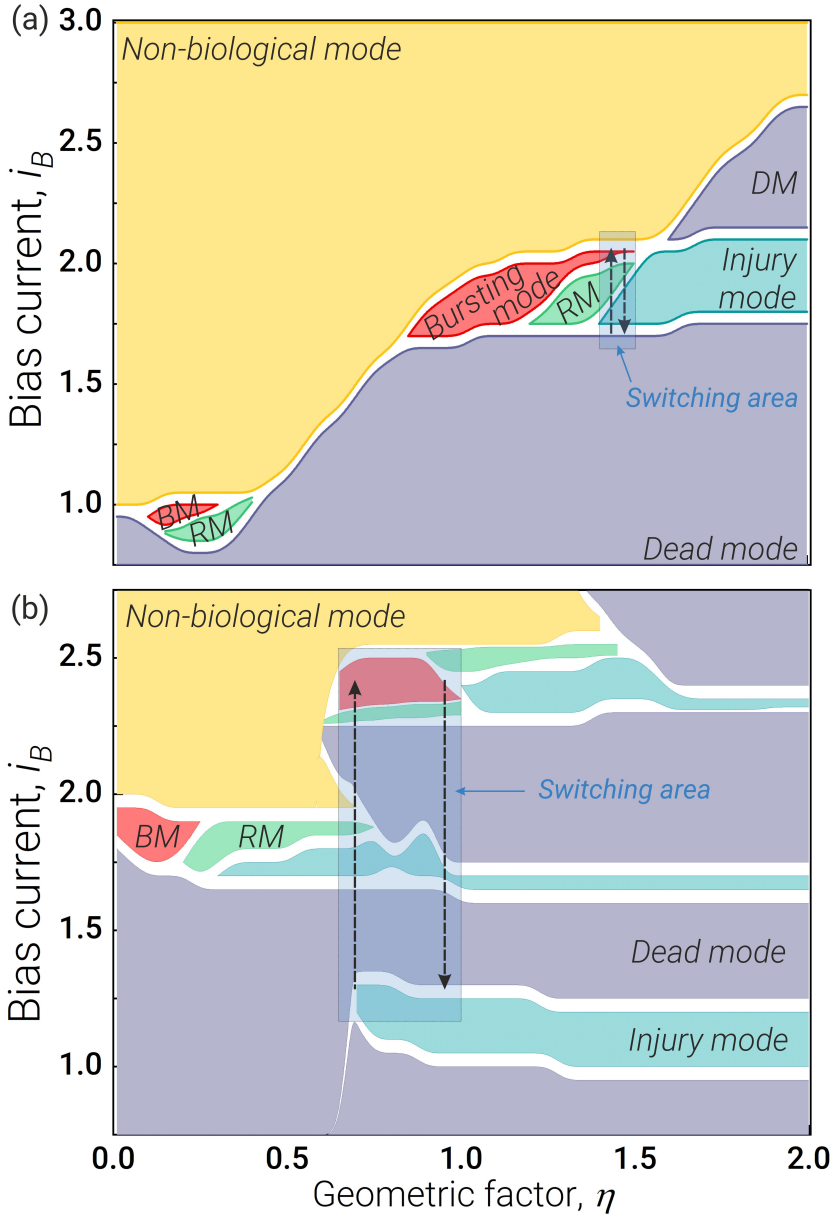


Figure 3. Parameter ranges for the operating modes of the neurons for the bias current i_b (which can be adjusted in situ) and the geometric factor η for (**a**) the $2JJ$ neuron (see Figure 1a) and (**b**) the $3JJ$ neuron (see Figure 1b). The parameters of the $2JJ$ neuron are $l_S = l_P = 5$, $\Gamma = 0.65$. The parameters of the $3JJ$ neuron are $l_S = 3.85$, $l = 5$, $\Gamma = 0.8$. The neuron was excited by rectangular pulses with level $A_{input} = 0.5$ and pulse duration $\tau = 20t_P$. The *switching area* highlighted by blue shows the range in which we can switch between all operating modes by adjusting the bias current i_b.

3. Synapse and Axon

Besides the development of a neuron, it is important to provide a mechanism for transferring excitation (action potential) from one neuron to another [78], with the effect of synaptic memory or synaptic plasticity—*short-term potentiation*. External stimulation of the presynaptic neuron should be able to either excite or inhibit the spike activity of the postsynaptic neuron, depending on the synaptic connection between them. The signal transfer through the synapse depends on its history: the more often the excitatory signal comes, the more it is transmitted.

The biosimilar model of an axon is a Josephson transmission line (JTL shown schematically in Figure 4a) [79], which is a parallel array of inductively coupled Josephson junctions

that transmit spikes corresponding to moving magnetic flux quanta. The equations for the axon JTL have a simple form:

$$\begin{cases} i_{a(1)} = i_{ba} - \frac{\phi_{a(1)} - \phi_{a(2)}}{l_a} + (i_{in})_{JTL}, \\ i_{a(2)} = i_{ba} + \frac{\phi_{a(1)} - 2\phi_{a(2)} + \phi_{a(3)}}{l_a}, \\ \ldots \\ i_{a(n)} = i_{ba} + \frac{\phi_{a(n-1)} - 2\phi_{a(n)} + \phi_{a(n+1)}}{l_a}, \\ \ldots \\ i_{a(N)} = i_{ba} - \frac{\phi_{a(N-1)} - \phi_{a(N)}}{l_a} - (i_{out})_{JTL}. \end{cases} \quad (8)$$

Here, i_{ba} is a bias current applied to each Josephson junction, $\phi_{a(n)}$ is a phase of the n-th Josephson junction, and l_a is a normalised coupling inductance. The current $i_{a(n)}$ flowing through the n-th Josephson junction is

$$i_{a(n)} = \ddot{\phi}_{a(n)} + \Gamma_a \dot{\phi}_{a(n)} + \sin \phi_{a(n)}, \quad (9)$$

where Γ_a is the damping parameter. Every JJ in the JTL has a critical current equal to that of the pulse JJ in the neuron. Note that certain myelin sheath properties of biological axons can be modelled by adjusting the value of the coupling inductance l_a and parameters of Josephson junctions $JJ_{a(n)}$.

A superconducting synapse is usually an *RLC*-circuit [47], see Figure 4b, where the high-frequency current is grounded through capacitance C_{syn}, while resistance R_{12} is used to prevent the bias current outflow from the postsynaptic neuron. The possibility of implementing an excitatory and inhibitory synaptic connection based on such a circuit has already been demonstrated. However, analysis of the amplitude–frequency characteristic shows that it is impossible to model the synaptic plasticity mentioned above using such an *RLC* filter (see Figure 5).

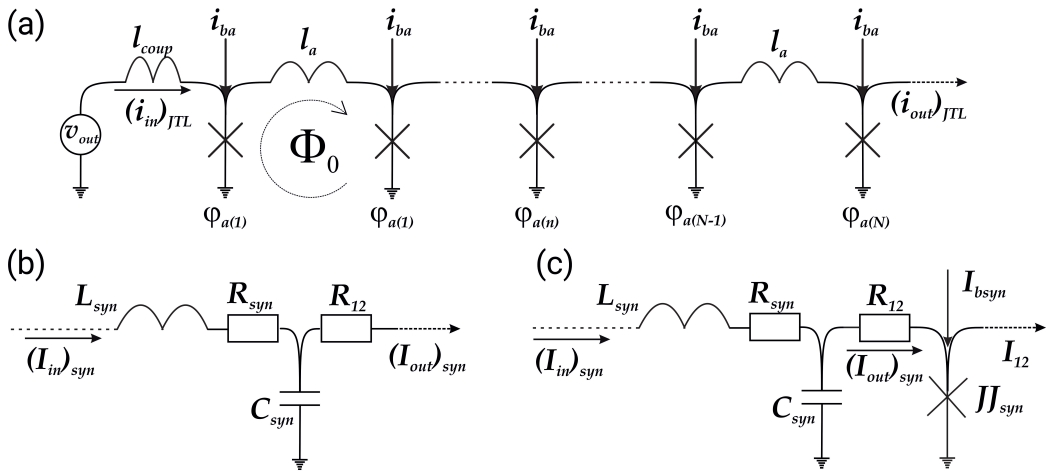


Figure 4. Schematic representation of (**a**) Josephson transmission line and synapses: (**b**) conventional design [47] and (**c**) modified *RLCJ*-synapse with additional Josephson junction connected in parallel to the *RLC*-filter.

We propose a modified design of the synapse to capture the short-term potentiation property of its biological counterpart. To suppress the low-frequency current, we add a

Josephson junction as shown in Figure 4c. Equations for the obtained *RLCJ* synapse are as follows:

$$\begin{cases} \ddot{v}_{syn} = \omega_0^2 \cdot \left\{ -\frac{Q}{\omega_0}\dot{v}_{syn} - v_{syn} + (v_{in})_{syn} - \left[l_{syn} \cdot \frac{d}{dt} + Q\omega_0 l_{syn} \right] \cdot (i_{out})_{syn} \right\}, \\ (i_{out})_{syn} = \frac{\Gamma}{r_{12}} \cdot (v_{syn} - v_{JJsyn}), \\ v_{JJsyn} = \dot{\phi}_{JJsyn}, \\ \ddot{\phi}_{JJsyn} = i_{bsyn} + (i_{out})_{syn} - i_{12} - \Gamma_{JJsyn}\dot{\phi}_{JJsyn} - \sin\phi_{JJsyn}, \\ \frac{(i_{out})_{syn}}{dt} = \frac{\Gamma}{r_{12}} \cdot \left\{ \dot{v}_{syn} - i_{bsyn} - (i_{out})_{syn} + i_{12} + \Gamma_{JJsyn}\dot{\phi}_{JJsyn} + \sin\phi_{JJsyn} \right\}, \end{cases} \tag{10}$$

where the abbreviation JJ_{syn} stands for the synaptic Josephson junction, JJ_{syn}; ω_0, Q, and l_{syn} are the resonant frequency, quality factor and inductance of the RLC-filter, respectively; r_{12} is a coupling resistance between the *RLC* part of the synapse and its Josephson junction; and i_{bsyn} is a synaptic bias current. The resulting *RLCJ* synapse changes the repetition frequency of the passing pulses proportional to this frequency, see Figure 5. The higher the frequency at the input, the greater the number of spikes at the output.

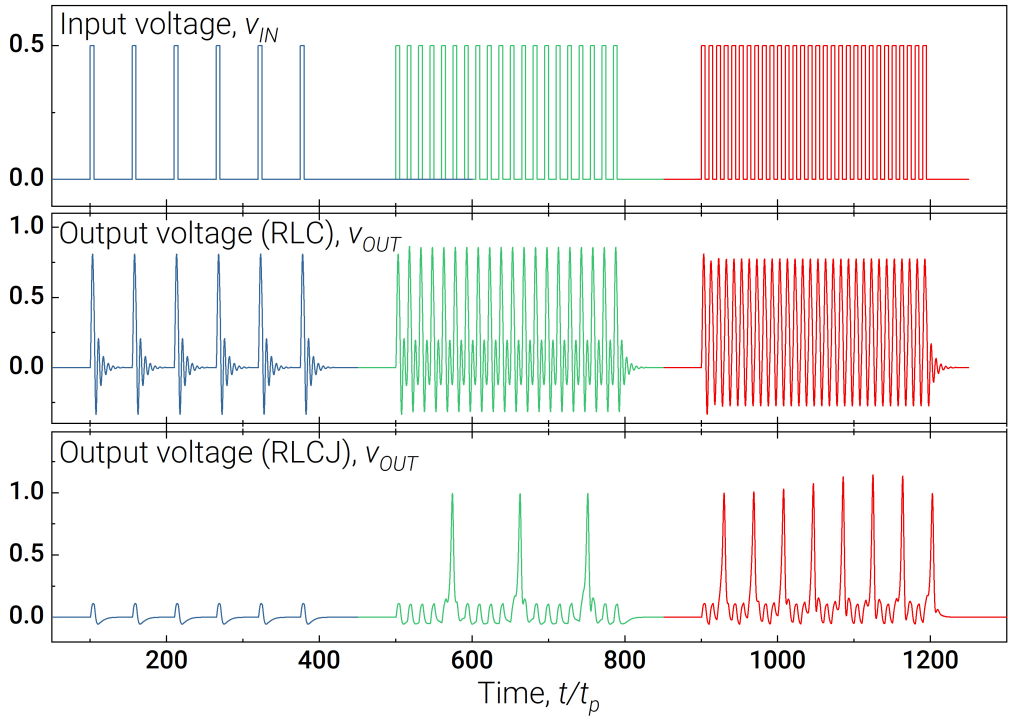


Figure 5. Illustration of one-to-one spike transfer with the conventional *RLC* synaptic model (proposed in the [47] by P. Crotty et al.) and synaptic plasticity obtained with the modified *RLCJ* model. The colour of the curves indicates their belonging to the one group consisting of a sequence of input voltage pulses, as well as responses for *RLC* and *RLCJ* synapse. The input voltage pulses are the same in both cases and have level $A_{input} = 0.5$ and pulse duration $\tau = 5t_p$. The system parameters are $l_{syn} = 2.655$, $Q = 0.3$, $\omega_0 = 1$, $r_{12} = 1.2$, $\Gamma_{JJsyn} = \Gamma = 1.4$, $i_{bsyn} = 0.9$. Both synaptic models were clocked with a series of voltage pulses (the duration of the series was the same each time) with an inter-pulse delay $5t_p$, $10t_p$ and $50t_p$.

4. Two-Neuron Chain

We also simulated two neurons connected through the axon and synapse (see Figure 6a). For this simple network architecture, we used the developed $3JJ$-neuron model, a JTL as an axon and a modified *RLCJ* circuit as a synapse. Figure 6b demonstrates the correct operation of the studied circuit in the considered modes. The postsynaptic neuron is connected here to the circuit with the synapse via the resistor R_a to eliminate the possibility of parasitic backaction.

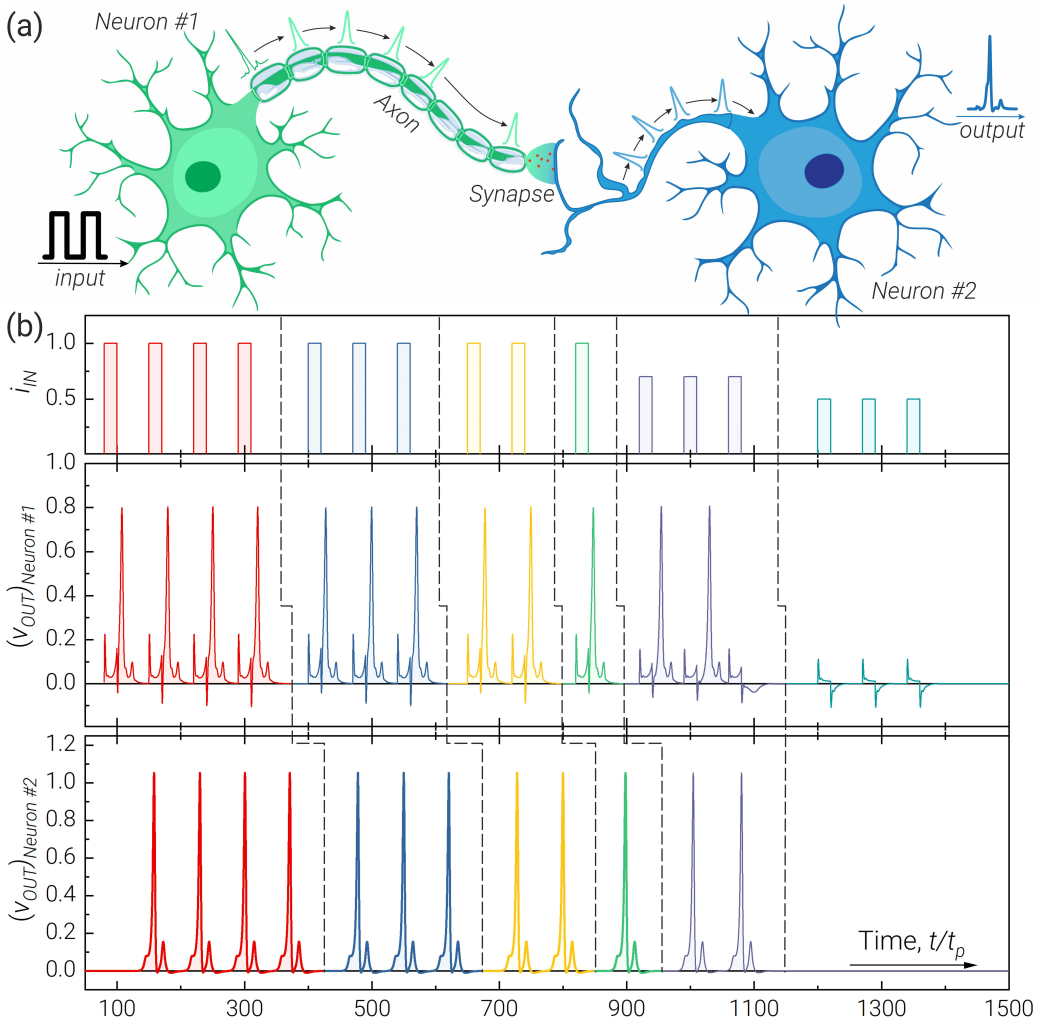


Figure 6. Illustration of a two-neuron chain operation composed of two $3JJ$ neurons, JTL as an axon, and a *RLCJ*-synapse. (**a**) Biosimilar sketch of the system. (**b**) Output pulses of excitatory (*Neuron* #1) and postsynaptic (*Neuron* #2) neurons for different levels and numbers of the input signals, i_{in}. Parameters of the system: $l = 5$, $l_S = 3.85$, $l_{SQ} = l + l_S$, $i_b = 1.9$, $\Gamma = 1.4$, $\eta = 0.2$; $l_{coup} = 1$, $i_{bA} = 0.95$, $l_A = 0.3 l_{SQ}$, $\Gamma_A = 2$, number of JJ in the JTL $= 10$, $r_a = 1.2$; $l_{syn} = l_A$, $\omega_0 = 1$, $Q = 0.3$, $r_{12} = 1.2$, $\Gamma_{JJsyn} = 1.4$, $i_{bsyn} = 0.9$.

From the results of the simulation shown in Figure 6, it is clear that there is potential for the Josephson excitatory neuron to function efficiently. However, in the real brain, inhibitory neurons also play an important role. In order to further develop the research presented, it is necessary to demonstrate the functioning of an inhibitory neuron in a system consisting of at least three neurons (excitatory, inhibitory and target neuron).

5. Conclusions

In this work, we explored new bio-inspired modes of operation of a conventional $2JJ$ superconducting model of a biological neuron. We described the analogy between the operation of the sodium–potassium pump and the dynamics of magnetic flux penetration in a superconducting circuit with Josephson junctions. We showed for the first time that it is possible to switch between the operating modes in situ by adjusting the bias current of the circuit. The use of the modified $3JJ$ biosimilar neuron provides a significant increase in the parameter margins of the switching area. We also studied the transfer function of the conventional synaptic *RLC*-model. We proposed its *RLCJ* modification to mimic the synaptic plasticity, i.e., the short-term potentiation of a biological synapse. Finally, we simulated the simplest two-neuron chain composed of $3JJ$ neurons, *RLCJ*-synapse and

axons modelled by JTLs. Its correct operation in the considered modes is demonstrated. Optimisation at the architectural level and experimental implementation of the networks modelling neural tissue are the next step in this field of research. Another important direction for extending the applicability of superconducting hardware models is to mimic other types of synaptic plasticity, such as spike-timing-dependent [59] and long-term plasticity. Together with addressing the issue of the down-scaling of superconducting circuits, e.g., by pursuing the inductor-less approach [80,81], these efforts are paving the way for the fast and energy-efficient hardware embodiment of artificial intelligence.

Author Contributions: Conceptualisation, A.E.S., N.V.K. and I.I.S.; Data curation, N.V.K.; Formal analysis, N.V.K.; Methodology, A.E.S.; Software, A.E.S. and G.I.G.; Supervision, M.Y.K.; Validation, I.I.S. and M.Y.K.; Visualisation, A.E.S.; Writing—original draft, A.E.S. and N.V.K.; Writing—review and editing, I.I.S. with contribution from the coauthors. All authors have read and agreed to the published version of the manuscript.

Funding: The development of the numerical simulation algorithm is supported by Grant No. 20-12-00130 https://rscf.ru/project/20-12-00130/ (accessed on 14 June 2023). The concept design was supported by UNN within the framework of the strategic academic leadership programme "Priority 2030" of the Ministry of Science and Higher Education of the Russian Federation. A.S. is grateful to the grant 22-1-3-16-1 from the Foundation for the Advancement of Theoretical Physics and Mathematics "BASIS".

Institutional Review Board Statement: Not applicable.

Data Availability Statement: All relevant data are included in the article.

Acknowledgments: We would like to express our gratitude to Ivan Nazhestkin for his invaluable assistance in developing methods for modelling the dynamics of Josephson bio-neurons and synapses.

Conflicts of Interest: The authors declare no conflict of interest. The funders had no role in the design of the study; in the collection, analyses, or interpretation of data; in the writing of the manuscript; or in the decision to publish the results.

References

1. Padamsey, Z.; Katsanevaki, D.; Dupuy, N.; Rochefort, N.L. Neocortex saves energy by reducing coding precision during food scarcity. *Neuron* **2022**, *110*, 280–296. [CrossRef] [PubMed]
2. LaBar, K.S.; Gitelman, D.R.; Parrish, T.B.; Kim, Y.H.; Nobre, A.C.; Mesulam, M. Hunger selectively modulates corticolimbic activation to food stimuli in humans. *Behav. Neurosci.* **2001**, *115*, 493. [CrossRef]
3. Fisher, M.P. Quantum cognition: The possibility of processing with nuclear spins in the brain. *Ann. Phys.* **2015**, *362*, 593–602. [CrossRef]
4. Hamilos, A.E.; Spedicato, G.; Hong, Y.; Sun, F.; Li, Y.; Assad, J.A. Slowly evolving dopaminergic activity modulates the moment-to-moment probability of reward-related self-timed movements. *Elife* **2021**, *10*, e62583. [CrossRef]
5. Hudspeth, A. How hearing happens. *Neuron* **1997**, *19*, 947–950. [CrossRef]
6. Schneider, D.M.; Mooney, R. How movement modulates hearing. *Annu. Rev. Neurosci.* **2018**, *41*, 553. [CrossRef]
7. Brouwer, G.J.; Heeger, D.J. Decoding and reconstructing color from responses in human visual cortex. *J. Neurosci.* **2009**, *29*, 13992–14003. [CrossRef]
8. Saygin, Z.M.; Osher, D.E.; Norton, E.S.; Youssoufian, D.A.; Beach, S.D.; Feather, J.; Gaab, N.; Gabrieli, J.D.; Kanwisher, N. Connectivity precedes function in the development of the visual word form area. *Nat. Neurosci.* **2016**, *19*, 1250–1255. [CrossRef] [PubMed]
9. Lutas, A.; Kucukdereli, H.; Alturkistani, O.; Carty, C.; Sugden, A.U.; Fernando, K.; Diaz, V.; Flores-Maldonado, V.; Andermann, M.L. State-specific gating of salient cues by midbrain dopaminergic input to basal amygdala. *Nat. Neurosci.* **2019**, *22*, 1820–1833. [CrossRef]
10. Tansley, S.; Gu, N.; Guzmán, A.U.; Cai, W.; Wong, C.; Lister, K.C.; Muñoz-Pino, E.; Yousefpour, N.; Roome, R.B.; Heal, J.; et al. Microglia-mediated degradation of perineuronal nets promotes pain. *Science* **2022**, *377*, 80–86. [CrossRef]
11. Roy, D.S.; Park, Y.G.; Kim, M.E.; Zhang, Y.; Ogawa, S.K.; DiNapoli, N.; Gu, X.; Cho, J.H.; Choi, H.; Kamentsky, L.; et al. Brain-wide mapping reveals that engrams for a single memory are distributed across multiple brain regions. *Nat. Commun.* **2022**, *13*, 1799. [CrossRef]
12. DeBole, M.V.; Taba, B.; Amir, A.; Akopyan, F.; Andreopoulos, A.; Risk, W.P.; Kusnitz, J.; Otero, C.O.; Nayak, T.K.; Appuswamy, R.; et al. TrueNorth: Accelerating from zero to 64 million neurons in 10 years. *Computer* **2019**, *52*, 20–29. [CrossRef]
13. Arute, F.; Arya, K.; Babbush, R.; Bacon, D.; Bardin, J.C.; Barends, R.; Biswas, R.; Boixo, S.; Brandao, F.G.; Buell, D.A.; et al. Quantum supremacy using a programmable superconducting processor. *Nature* **2019**, *574*, 505–510. [CrossRef]

14. Davies, M.; Srinivasa, N.; Lin, T.H.; Chinya, G.; Cao, Y.; Choday, S.H.; Dimou, G.; Joshi, P.; Imam, N.; Jain, S.; et al. Loihi: A neuromorphic manycore processor with on-chip learning. *IEEE Micro* **2018**, *38*, 82–99. [CrossRef]
15. Kumar, S. Introducing Qualcomm Zeroth Processors: Brain-Inspired Computing. *Qualcomm OnQ Blog*, 2013; pp. 1–11. Available online: https://www.qualcomm.com/news/onq/2013/10/introducing-qualcomm-zeroth-processors-brain-inspired-computing (accessed on 1 January 2020).
16. Prezioso, M.; Merrikh-Bayat, F.; Hoskins, B.; Adam, G.C.; Likharev, K.K.; Strukov, D.B. Training and operation of an integrated neuromorphic network based on metal-oxide memristors. *Nature* **2015**, *521*, 61–64. [CrossRef]
17. Bose, S.K.; Mallinson, J.B.; Gazoni, R.M.; Brown, S.A. Stable self-assembled atomic-switch networks for neuromorphic applications. *IEEE Trans. Electron Devices* **2017**, *64*, 5194–5201. [CrossRef]
18. Wan, W.; Kubendran, R.; Schaefer, C.; Eryilmaz, S.B.; Zhang, W.; Wu, D.; Deiss, S.; Raina, P.; Qian, H.; Gao, B.; et al. A compute-in-memory chip based on resistive random-access memory. *Nature* **2022**, *608*, 504–512. [CrossRef] [PubMed]
19. Lowery, A.J.; Rosenfeld, J.V.; Lewis, P.M.; Browne, D.; Mohan, A.; Brunton, E.; Yan, E.; Maller, J.; Mann, C.; Rajan, R.; et al. Restoration of vision using wireless cortical implants: The Monash Vision Group project. In Proceedings of the 2015 37th Annual International Conference of the IEEE Engineering in Medicine and Biology Society (EMBC), Milan, Italy, 25–29 August 2015; IEEE: New York, NY, USA, 2015; pp. 1041–1044.
20. Roska, B.; Sahel, J.A. Restoring vision. *Nature* **2018**, *557*, 359–367. [CrossRef]
21. Yue, L.; Wuyyuru, V.; Gonzalez-Calle, A.; Dorn, J.D.; Humayun, M.S. Retina–electrode interface properties and vision restoration by two generations of retinal prostheses in one patient—One in each eye. *J. Neural Eng.* **2020**, *17*, 026020. [CrossRef]
22. Litovsky, R.Y.; Moua, K.; Godar, S.; Kan, A.; Misurelli, S.M.; Lee, D.J. Restoration of spatial hearing in adult cochlear implant users with single-sided deafness. *Hear. Res.* **2019**, *372*, 69–79. [CrossRef] [PubMed]
23. Muller, L.; Gilbert, M.; Jiam, N.T.; Limb, C.J.; Tward, A.D. Electrical Determinants of Tinnitus Extinction in a Cochlear Implant Patient. *Otol. Neurotol.* **2022**, *44*, e8–e12. [CrossRef] [PubMed]
24. Wang, B.; Yang, H.; Chen, X. Cochlear implant technology: Previous, present and future. *Wearable Technol.* **2022**, *3*, 112–124.
25. Mansour, A.A.; Gonçalves, J.T.; Bloyd, C.W.; Li, H.; Fernandes, S.; Quang, D.; Johnston, S.; Parylak, S.L.; Jin, X.; Gage, F.H. An in vivo model of functional and vascularized human brain organoids. *Nat. Biotechnol.* **2018**, *36*, 432–441. [CrossRef]
26. Beniaguev, D.; Segev, I.; London, M. Single cortical neurons as deep artificial neural networks. *Neuron* **2021**, *109*, 2727–2739. [CrossRef] [PubMed]
27. Millet, J.; Caucheteux, C.; Orhan, P.; Boubenec, Y.; Gramfort, A.; Dunbar, E.; Pallier, C.; King, J.R. Toward a realistic model of speech processing in the brain with self-supervised learning. *arXiv* **2022**, arXiv:2206.01685.
28. Bakhtiari, S.; Mineault, P.; Lillicrap, T.; Pack, C.; Richards, B. The functional specialization of visual cortex emerges from training parallel pathways with self-supervised predictive learning. *Adv. Neural Inf. Process. Syst.* **2021**, *34*, 25164–25178.
29. Kell, A.J.; Yamins, D.L.; Shook, E.N.; Norman-Haignere, S.V.; McDermott, J.H. A task-optimized neural network replicates human auditory behavior, predicts brain responses, and reveals a cortical processing hierarchy. *Neuron* **2018**, *98*, 630–644. [CrossRef]
30. Kell, A.J.; McDermott, J.H. Deep neural network models of sensory systems: Windows onto the role of task constraints. *Curr. Opin. Neurobiol.* **2019**, *55*, 121–132. [CrossRef] [PubMed]
31. Jones, I.S.; Kording, K.P. Do biological constraints impair dendritic computation? *Neuroscience* **2022**, *489*, 262–274. [CrossRef] [PubMed]
32. Eslami, S.A.; Jimenez Rezende, D.; Besse, F.; Viola, F.; Morcos, A.S.; Garnelo, M.; Ruderman, A.; Rusu, A.A.; Danihelka, I.; Gregor, K.; et al. Neural scene representation and rendering. *Science* **2018**, *360*, 1204–1210. [CrossRef]
33. Willett, F.R.; Avansino, D.T.; Hochberg, L.R.; Henderson, J.M.; Shenoy, K.V. High-performance brain-to-text communication via handwriting. *Nature* **2021**, *593*, 249–254. [CrossRef] [PubMed]
34. Shapson-Coe, A.; Januszewski, M.; Berger, D.R.; Pope, A.; Wu, Y.; Blakely, T.; Schalek, R.L.; Li, P.H.; Wang, S.; Maitin-Shepard, J.; et al. A connectomic study of a petascale fragment of human cerebral cortex. *BioRxiv* **2021**. [CrossRef]
35. Adam, E.M.; Johns, T.; Sur, M. Dynamic control of visually guided locomotion through corticosubthalamic projections. *Cell Rep.* **2022**, *40*, 111139. [CrossRef]
36. Liu, X.; Huang, H.; Snutch, T.P.; Cao, P.; Wang, L.; Wang, F. The Superior Colliculus: Cell Types, Connectivity, and Behavior. *Neurosci. Bull.* **2022**, *38*, 1519–1540. [CrossRef] [PubMed]
37. Jiang, X.; Pan, Y. Neural Control of Action Selection Among Innate Behaviors. *Neurosci. Bull.* **2022**, *38*, 1541–1558. [CrossRef] [PubMed]
38. Maass, W. Networks of spiking neurons: The third generation of neural network models. *Neural Netw.* **1997**, *10*, 1659–1671. [CrossRef]
39. Ponulak, F.; Kasinski, A. Introduction to spiking neural networks: Information processing, learning and applications. *Acta Neurobiol. Exp.* **2011**, *71*, 409–433.
40. Schliebs, S.; Kasabov, N. Evolving spiking neural network—A survey. *Evol. Syst.* **2013**, *4*, 87–98. [CrossRef]
41. Indiveri, G.; Linares-Barranco, B.; Hamilton, T.J.; Schaik, A.v.; Etienne-Cummings, R.; Delbruck, T.; Liu, S.C.; Dudek, P.; Häfliger, P.; Renaud, S.; et al. Neuromorphic silicon neuron circuits. *Front. Neurosci.* **2011**, *5*, 73. [CrossRef]
42. Han, J.K.; Oh, J.; Yun, G.J.; Yoo, D.; Kim, M.S.; Yu, J.M.; Choi, S.Y.; Choi, Y.K. Cointegration of single-transistor neurons and synapses by nanoscale CMOS fabrication for highly scalable neuromorphic hardware. *Sci. Adv.* **2021**, *7*, eabg8836. [CrossRef]
43. Jeong, H.; Shi, L. Memristor devices for neural networks. *J. Phys. D Appl. Phys.* **2018**, *52*, 023003. [CrossRef]

44. Berggren, K.; Xia, Q.; Likharev, K.K.; Strukov, D.B.; Jiang, H.; Mikolajick, T.; Querlioz, D.; Salinga, M.; Erickson, J.R.; Pi, S.; et al. Roadmap on emerging hardware and technology for machine learning. *Nanotechnology* **2020**, *32*, 012002. [CrossRef] [PubMed]
45. Feldmann, J.; Youngblood, N.; Wright, C.D.; Bhaskaran, H.; Pernice, W.H. All-optical spiking neurosynaptic networks with self-learning capabilities. *Nature* **2019**, *569*, 208–214. [CrossRef] [PubMed]
46. Jha, A.; Huang, C.; Peng, H.T.; Shastri, B.; Prucnal, P.R. Photonic spiking neural networks and CMOS-compatible graphene-on-silicon spiking neurons. *arXiv* **2021**, arXiv:2109.13797.
47. Crotty, P.; Schult, D.; Segall, K. Josephson junction simulation of neurons. *Phys. Rev. E* **2010**, *82*, 011914. [CrossRef]
48. Russek, S.E.; Donnelly, C.A.; Schneider, M.L.; Baek, B.; Pufall, M.R.; Rippard, W.H.; Hopkins, P.F.; Dresselhaus, P.D.; Benz, S.P. Stochastic single flux quantum neuromorphic computing using magnetically tunable Josephson junctions. In Proceedings of the 2016 IEEE International Conference on Rebooting Computing (ICRC), San Diego, CA, USA, 17–19 October 2016; IEEE: New York, NY, USA, 2016; pp. 1–5.
49. Schegolev, A.E.; Klenov, N.V.; Soloviev, I.I.; Tereshonok, M.V. Adiabatic superconducting cells for ultra-low-power artificial neural networks. *Beilstein J. Nanotechnol.* **2016**, *7*, 1397–1403. [CrossRef]
50. Soloviev, I.I.; Schegolev, A.E.; Klenov, N.V.; Bakurskiy, S.V.; Kupriyanov, M.Y.; Tereshonok, M.V.; Shadrin, A.V.; Stolyarov, V.S.; Golubov, A.A. Adiabatic superconducting artificial neural network: Basic cells. *J. Appl. Phys.* **2018**, *124*, 152113. [CrossRef]
51. Cheng, R.; Goteti, U.S.; Hamilton, M.C. Spiking neuron circuits using superconducting quantum phase-slip junctions. *J. Appl. Phys.* **2018**, *124*, 152126. [CrossRef]
52. Schneider, M.L.; Donnelly, C.A.; Russek, S.E.; Baek, B.; Pufall, M.R.; Hopkins, P.F.; Dresselhaus, P.D.; Benz, S.P.; Rippard, W.H. Ultralow power artificial synapses using nanotextured magnetic Josephson junctions. *Sci. Adv.* **2018**, *4*, e1701329. [CrossRef]
53. Toomey, E.; Segall, K.; Castellani, M.; Colangelo, M.; Lynch, N.; Berggren, K.K. Superconducting nanowire spiking element for neural networks. *Nano Lett.* **2020**, *20*, 8059–8066. [CrossRef]
54. Schegolev, A.; Klenov, N.; Soloviev, I.; Tereshonok, M. Learning cell for superconducting neural networks. *Supercond. Sci. Technol.* **2020**, *34*, 015006. [CrossRef]
55. Zhang, H.; Gang, C.; Xu, C.; Gong, G.; Lu, H. Brain-inspired spiking neural network using superconducting devices. *IEEE Trans. Emerg. Top. Comput. Intell.* **2021**, *7*, 271–277. [CrossRef]
56. Semenov, V.K.; Golden, E.B.; Tolpygo, S.K. A new family of bioSFQ logic/memory cells. *IEEE Trans. Appl. Supercond.* **2021**, *32*, 1–5. [CrossRef]
57. Casaburi, A.; Hadfield, R.H. Superconducting circuits that mimic the brain. *Nat. Electron.* **2022**, *5*, 627–628. [CrossRef]
58. Schneider, M.; Toomey, E.; Rowlands, G.; Shainline, J.; Tschirhart, P.; Segall, K. SuperMind: A survey of the potential of superconducting electronics for neuromorphic computing. *Supercond. Sci. Technol.* **2022**, *35*, 053001. [CrossRef]
59. Segall, K.; Purmessur, C.; D'Addario, A.; Schult, D. A superconducting synapse exhibiting spike-timing dependent plasticity. *Appl. Phys. Lett.* **2023**, *122*, 242601. [CrossRef]
60. Widdows, D.; Rani, J.; Pothos, E.M. Quantum circuit components for cognitive decision-making. *Entropy* **2023**, *25*, 548. [CrossRef] [PubMed]
61. Vozhakov, V.A.; Bastrakova, M.V.; Klenov, N.V.; Soloviev, I.I.; Pogosov, W.V.; Babukhin, D.V.; Zhukov, A.A.; Satanin, A.M. State control in superconducting quantum processors. *Phys.-Uspekhi* **2022**, *65*, 457–476. [CrossRef]
62. Skryabina, O.V.; Schegolev, A.E.; Klenov, N.V.; Bakurskiy, S.V.; Shishkin, A.G.; Sotnichuk, S.V.; Napolskii, K.S.; Nazhestkin, I.A.; Soloviev, I.I.; Kupriyanov, M.Y.; et al. Superconducting Bio-Inspired Au-Nanowire-Based Neurons. *Nanomaterials* **2022**, *12*, 1671. [CrossRef]
63. Soloviev, I.; Klenov, N.; Schegolev, A.; Bakurskiy, S.; Kupriyanov, M.Y. Analytical derivation of DC SQUID response. *Supercond. Sci. Technol.* **2016**, *29*, 094005. [CrossRef]
64. Hodgkin, A.L.; Huxley, A.F. Propagation of electrical signals along giant nerve fibres. *Proc. R. Soc. Lond. Ser. B-Biol. Sci.* **1952**, *140*, 177–183.
65. Lisman, J.E. Bursts as a unit of neural information: Making unreliable synapses reliable. *Trends Neurosci.* **1997**, *20*, 38–43. [CrossRef] [PubMed]
66. Selig, D.K.; Nicoll, R.A.; Malenka, R.C. Hippocampal long-term potentiation preserves the fidelity of postsynaptic responses to presynaptic bursts. *J. Neurosci.* **1999**, *19*, 1236–1246. [CrossRef] [PubMed]
67. Elson, R.C.; Selverston, A.I.; Huerta, R.; Rulkov, N.F.; Rabinovich, M.I.; Abarbanel, H.D. Synchronous behavior of two coupled biological neurons. *Phys. Rev. Lett.* **1998**, *81*, 5692. [CrossRef]
68. Elson, R.C.; Selverston, A.I.; Abarbanel, H.D.; Rabinovich, M.I. Inhibitory synchronization of bursting in biological neurons: Dependence on synaptic time constant. *J. Neurophysiol.* **2002**, *88*, 1166–1176. [CrossRef]
69. Pauls, K.A.M.; Korsun, O.; Nenonen, J.; Nurminen, J.; Liljeström, M.; Kujala, J.; Pekkonen, E.; Renvall, H. Cortical beta burst dynamics are altered in Parkinson's disease but normalized by deep brain stimulation. *NeuroImage* **2022**, *257*, 119308. [CrossRef]
70. Brofiga, M.; Pisano, M.; Raiteri, R.; Massobrio, P. On the road to the brain-on-a-chip: A review on strategies, methods, and applications. *J. Neural Eng.* **2021**, *18*, 041005. [CrossRef]
71. Gray, C.M.; McCormick, D.A. Chattering cells: Superficial pyramidal neurons contributing to the generation of synchronous oscillations in the visual cortex. *Science* **1996**, *274*, 109–113. [CrossRef]
72. Izhikevich, E.M.; Desai, N.S.; Walcott, E.C.; Hoppensteadt, F.C. Bursts as a unit of neural information: Selective communication via resonance. *Trends Neurosci.* **2003**, *26*, 161–167. [CrossRef]

73. Cattaneo, A.; Maffei, L.; Morrone, C. Patterns in the discharge of simple and complex visual cortical cells. *Proc. R. Soc. Lond. Ser. B. Biol. Sci.* **1981**, *212*, 279–297.
74. Otto, T.; Eichenbaum, H.; Wible, C.G.; Wiener, S.I. Learning-related patterns of CA1 spike trains parallel stimulation parameters optimal for inducing hippocampal long-term potentiation. *Hippocampus* **1991**, *1*, 181–192. [CrossRef] [PubMed]
75. Williams, S.R.; Stuart, G.J. Mechanisms and consequences of action potential burst firing in rat neocortical pyramidal neurons. *J. Physiol.* **1999**, *521*, 467. [CrossRef] [PubMed]
76. Fabian, J.M.; Wiederman, S.D. Spike bursting in a dragonfly target-detecting neuron. *Sci. Rep.* **2021**, *11*, 4005. [CrossRef]
77. West, J.T.; Kurlej, A.; Wynn, A.; Rogers, C.; Gouker, M.A.; Tolpygo, S.K. Wafer-Scale Characterization of a Superconductor Integrated Circuit Fabrication Process, Using a Cryogenic Wafer Prober. *IEEE Trans. Appl. Supercond.* **2022**, *32*, 9500712. [CrossRef]
78. Bullmore, E.; Sporns, O. Complex brain networks: Graph theoretical analysis of structural and functional systems. *Nat. Rev. Neurosci.* **2009**, *10*, 186–198. [CrossRef]
79. Feldhoff, F.; Toepfer, H. Niobium Neuron: RSFQ Based Bio-Inspired Circuit. *IEEE Trans. Appl. Supercond.* **2021**, *31*, 1800505. [CrossRef]
80. Soloviev, I.; Ruzhickiy, V.; Bakurskiy, S.; Klenov, N.; Kupriyanov, M.Y.; Golubov, A.; Skryabina, O.; Stolyarov, V. Superconducting circuits without inductors based on bistable Josephson junctions. *Phys. Rev. Appl.* **2021**, *16*, 014052. [CrossRef]
81. Salameh, I.; Friedman, E.G.; Kvatinsky, S. Superconductive Logic Using 2ϕ—Josephson Junctions With Half Flux Quantum Pulses. *IEEE Trans. Circuits Syst. II Express Briefs* **2022**, *69*, 2533–2537. [CrossRef]

Disclaimer/Publisher's Note: The statements, opinions and data contained in all publications are solely those of the individual author(s) and contributor(s) and not of MDPI and/or the editor(s). MDPI and/or the editor(s) disclaim responsibility for any injury to people or property resulting from any ideas, methods, instructions or products referred to in the content.